Hydrophobic Helical Hairpins: Design and Packing Interactions in Membrane Environments†

Rachel M. Johnson, Claire L. Heslop, and Charles M. Deber*

Division of Structural Biology and Biochemistry, Research Institute, The Hospital for Sick Children, Toronto, Ontario M5G 1X8, and Department of Biochemistry, University of Toronto, Toronto, Ontario M5S 1A8, Canada

Received April 12, 2004; Revised Manuscript Received August 26, 2004

ABSTRACT: Helix−helix interactions within membranes are dominated by van der Waals packing motifs and side chain−side chain hydrogen bond formation, which act in tandem to determine the residues that comprise the interface between two given helices. To explore in a systematic manner the tertiary contacts between transmembrane helices, we have designed and expressed in *Escherichia coli* highly hydrophobic helix−loop−helix constructs of prototypic sequence K^{1}KKKKKKFAIAIAIIAWA**X**^{19}AIIAIAIAIKSPGSKIAIAIAIIA**Z**^{44}AWAIIAIAIAFKKKKKKK^{62}, where "small" (Ala) and "large" (Ile) residues were used to maximize the tertiary contact area. Evidence that the two transmembrane (TM) segments in the **AI** construct contain an interface conducive for folding into a hairpin structure was obtained from the results that (i) the single TM $\mathbf{AI_{pep}}$ peptide derived from the **AI** hairpin forms SDS-resistant dimers on PAGE gels and (ii) the corresponding sequence forms a strong dimer when examined in vivo in TOXCAT assays. Site-directed mutagenesis of **AI** hairpins was carried out to incorporate each of the 20 commonly occurring amino acids at **X** positions. Analysis on Western blots using an oligomerization assay in 12% NuPage−sodium dodecyl sulfate (SDS) indicated that mutants with **X** = E, D, Q, R, N, H, and K largely formed SDS-resistant dimers—which likely correspond to H-bonded four-helix bundles—while all the others (e.g., **X** = F, W, L, I, M, V, C, Y, A, T, S, G, and P) remained monomeric. Systematic studies of **X**/**Z** double mutants indicated that formation of hairpin dimers is the result of the disruption of stabilizing interactions between the antiparallel helices within the **AI** construct. The overall results suggest that, in situations where hydrophobic van der Waals packing energy between helices is sufficient to prevent significant rotation about the major axes of interacting helices, intrahairpin side chain−side chain H-bond formation will occur mainly when pairs of polar residues are interfacially located and proximal. Knowledge of the relative contributions of these forces should be of value, for example, in clarifying the context—and the structural consequences—of disease-related mutations.

Although membrane proteins are very abundant, only a few high-resolution structures have been determined (i.e., bacteriorhodopsin, photosynthetic reaction center, light-harvesting complex II, porin, hemolysin, and glycophorin A) (*1*). This paucity of structures is due, in part, to the highly hydrophobic nature of these proteins, which presents unique challenges to their handling and purification. Since the biological function of membrane proteins is related to how they fold and assemble, it is important to establish the principles that guide folding of proteins in membranes. Understanding packing motifs and the interactions among helices within membranes is therefore key to clarifying the context—and the molecular consequences—of a mutation; defects often lead to disease.

Membrane proteins are thought to fold in two steps (*2*, *3*). The first step involves independent insertion of individual helices into the membrane, a process driven mainly by the hydrophobic effect. De novo designed peptides have been previously used to characterize the helicity and hydrophobicity of individual α-helical transmembrane (TM)[1] segments (*1*). However, the second step involves the formation of tertiary contacts between transmembrane helices. Here, protein folding is driven fundamentally by van der Waals interactions, which are enhanced by favorable packing interactions between side chains (*4*, *5*). More recently, it has been reported that although occurrences of polar residues (such as Asp, Glu, Asn, and Gln) within TM segments are relatively few, electrostatic interactions likely play a major role in the folding of membrane proteins, wherein polar

† This work was supported, in part, by a grant to C.M.D. from the Canadian Institutes of Health Research (CIHR). R.M.J. held an Ontario Graduate Scholarship Award. C.L.H. was a participant in the Samuel B. Lunenfeld Summer Student Research Program at the Research Institute, Hospital for Sick Children.

* To whom correspondence should be addressed at The Hospital for Sick Children. Phone: (416) 813-5924. Fax: (416) 813-5005. E-mail: deber@sickkids.ca.

[1] Abbreviations: TM, transmembrane; H-bond, hydrogen bond; GpA, glycophorin A; IPTG, isopropyl 1-thio-β-D-galactoside; LB, Luria broth; Amp, ampicillin; SDS, sodium dodecyl sulfate; HRP, horseradish peroxidase; CD, circular dichroism; Trx, thioredoxin; CAT, chloramphenicol acetyltransferase; SDS−PAGE, sodium dodecyl sulfate−polyacrylamide gel electrophoresis; MBP, maltose-binding protein; FRET, fluorescence resonance energy transfer; dansyl, 5-dimethylaminonaphthalene-1-sulfonyl; dabsyl, 4-dimethylaminoazobenzene-4′-sulfonyl; Hsmr TM1, first transmembrane segment from the bacterial protein Hsmr; DIEA, *N*,*N*-diisopropylethylamine; DMF, *N*,*N*-dimethylformamide.

10.1021/bi0492760 CCC: $27.50 © 2004 American Chemical Society
Published on Web 10/21/2004

residues partner to form side chain−side chain hydrogen bonds between TM helices (*6*−*12*). Within the context of these considerations, strategically positioned residues in TM segments also play a central role in membrane protein folding. Several motifs have been reported which promote TM−TM segment packing, including the GxxxG motif (*13*) and multiple Ser/Thr motifs (SxxSSxxT and SxxxSSxxT) (*14*). Further, with the GxxxG grouping embedded, packing faces such as the glycophorin A dimerization motif (LIxxGVxxGVxxT) (*15*, *16*) and the bacteriophage M13 major coat protein dimerization motif (VVxxGAxxGIxxF) (*17*) have been elucidated. When examined in detail, these motifs apparently include combinations of specifically chosen residues—some forming side chain−side chain H-bonds, and some combinations of "large" and "small" (e.g., Gly) residues promoting helix−helix packing—but the question as to how certain residues "tune" the interfacial positioning and/or the relative affinity of pairs of helices within membranes is only beginning to be explored systematically (*18*). As well, the magnitudes and the relative importance of all of the forces contributing to helix−helix interactions have yet to be determined (*12*).

Previous studies have used homooligomeric TM proteins as model systems for exploring the thermodynamics of membrane protein folding, because of their symmetry and relative simplicity (*12*). Examples include glycophorin A (GpA) (*15*, *16*), the M2 proton channel from influenza A virus (M2), the M13 coat protein (*17*), and various designed systems (*1*, *7*, *8*, *10*, *11*). To examine residue-dependent tertiary contacts between pairs of helices in a membrane environment, we have now designed and expressed de novo constructs containing pairs of hydrophobic sequences of length comparable to that of membrane-spanning helices. When folded, these constructs resemble "helical hairpins", with residues such as Ile and Ala incorporated to promote "knobs-into-holes" interhelical packing characteristic of strong van der Waals interactions. A variable position was included in each helix (denoted **X** (Ile 19) and **Z** (Ile 44), respectively) such that the oligomeric state(s) resulting from both single and double substitutions—including polar residues—could be examined at these key positions.

EXPERIMENTAL PROCEDURES

Plasmid Construction. The **AI** hairpin sequence (Figure 1) was prepared by a mutually primed synthesis approach, using four primers of approximately 72−78 base pairs, with overlap regions of 33−36 base pairs. Two reactions were set up to create the first half and the second half of the **AI** hairpin sequence (consisting of 117 base pairs each). Each reaction involved annealing at an appropriate temperature of the two primers, followed by extension using Sequenase 2.0 (Amersham) and 10 mM dNTPs (Invitrogen). Subsequently, PCR (polymerize chain reaction) was used to join the two sections (a region of overlap between the two halves was included). This hairpin sequence was then cloned into the *Nco*I and *Xho*I sites of the pET32a(+) vector (Novagen) and transformed into BL21 (DE3) cells (Novagen).

*Expression, Extraction, and Thrombin Cleavage of **AI** Constructs for Oligomerization Assays.* All **AI** constructs were expressed as fusion proteins with thioredoxin (Trx), for increased solubility. For the expression of the constructs,

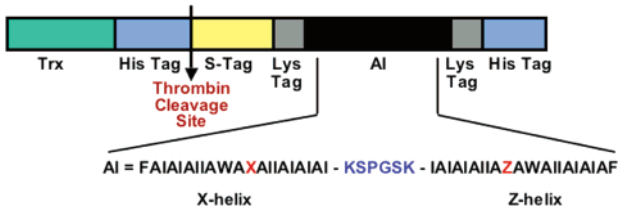

FIGURE 1: **AI** sequence (see the text) was cloned into the pET32a-(+) vector (Novagen) and is expressed as a fusion protein with thioredoxin. The **AI** sequence is comprised of two transmembrane helices (backbone residues Ala and Ile), linked by a soluble loop (KSPGSK), with Lys-tags incorporated on each end of the sequence to increase aqueous solubility during expression and purification steps. The superscripts 1 and 62 delineate the boundaries of the specific **AI** sequence and are used for residue numbering throughout. Note that the full **AI** hairpins studied by conformational and Western blot analysis in this work (Figures 2 and 4−6) contain all of the residues C-terminal to the thrombin cleavage site in the pET32a(+) vector, including an N-terminal S-tag and C-terminal His-tag (full sequence GSGMKETAAAKFERQHMDSPDL-GTDDDDKAMAK^{1}KKKKKKFAIAIAIIWA**X**AIIAIAIAIKSPG-SKIAIAIAIIA**Z**AWAIIAIAIAFKKKKKKK^{62}HHHHHHLE; 11122.4 Da, **X** = **Z** = Ile).

a single colony was inoculated with 30 mL of LB/Amp (Luria broth containing 100 μg/mL ampicillin) and grown at 37 °C and 250 rpm until A_{600} reached ~0.5. The culture was then induced with 0.1 mM IPTG (isopropyl 1-thio-β-D-galactoside) at 37 °C, and then grown for an additional 3 h at the induction temperature. Cells were separated into 1.5 mL aliquots and harvested by centrifugation at 13000 rpm for 2 min.

The harvested cell pellet (from a 1.5 mL culture containing the expressed thioredoxin−**AI** fusion protein) was resuspended in 300 μL of B-PER (bacterial protein extraction reagent) (Pierce), and was vortexed for 1 min at room temperature to lyse the cells. Then, the soluble and insoluble fractions were separated by centrifugation for 10 min at 13000 rpm. To the soluble fraction (containing thioredoxin−**AI** fusion protein) were added 0.1% Triton X-100, 5 mM $CaCl_2$, and 0.375 U/mL thrombin, and the mixture was agitated at room temperature for 3 h. This step allows for the removal of the thioredoxin fusion protein, resulting in the **AI** protein containing only an N-terminal S-tag (for Western blot identification purposes) and a C-terminal His-tag.

*SDS−PAGE and Western Blot Analysis of **X** and **X/Z** Mutants.* Gel boxes, gels, and buffers were purchased from Invitrogen, and PAGE was carried out according to the manufacturer's specifications. Two gel systems were used to examine the oligomerization of **X** and **X/Z** mutants: 12% NuPage−bis-tris and 4−20% Tris−glycine. The cleaved soluble fraction of each of the 20 **X** mutants (with **Z** = Ile), as well as several specific **X/Z** double mutants, was suspended in the appropriate sample buffers. Western blots were performed as per standard protocols, using an S-protein HRP-conjugate antibody (Novagen).

*Expression and Purification of the **AI** (**X/Z** = I/I) Construct.* The **AI** construct was expressed as described above, except that 500 mL of LB/Amp was used. The cells were harvested by centrifugation at 4000*g* for 20 min. The cell pellet was resuspended in 1/10 volume of lysis buffer (20 mM Tris−HCl, pH 8.0, containing 150 mM NaCl, 5 mM imidazole, and 0.1% Triton X-100) and sonicated. The lysate was centrifuged at 16 000*g* for 40 min.

All purification steps were performed at room temperature. The Trx−**AI** construct was purified from the lysis supernatant by nickel-chelate chromatography. The crude extract was incubated with 1/10 volume of resin for approximately 2 h. The resin was then washed with lysis buffer (containing 30 mM imidazole), and eluted with lysis buffer (containing 150 mM imidazole). The eluted fraction was cleaved with thrombin as described above, and purified further by reversed-phase high-performance liquid chromatography (RP-HPLC) using a C1 analytical column (Phenomenex) and a water/acetonitrile gradient (95:5 (v/v) to 5:95 (v/v) over 90 min at a flow rate of 1 mL/min). The fraction containing the **AI** construct was lyophilized, and used for Trp fluorescence and CD spectroscopy experiments.

Circular Dichroism (CD) Spectroscopy and Tryptophan Fluorescence. For CD spectroscopy, lyophilized protein was resuspended at a final concentration of 10 μM in 20 mM Tris−HCl, pH 8.0, or in 20 mM Tris−HCl, pH 8.0, containing 34 mM SDS. Samples were analyzed at room temperature, and the mean residue ellipticity (θ) was calculated as previously described (*19*).

For Trp fluorescence studies, lyophilized protein was resuspended at a final concentration of 2 μM in 20 mM Tris−HCl, pH 8.0, or in 20 mM Tris−HCl, pH 8.0, containing 6.8 mM SDS. Samples were analyzed at room temperature.

Peptide Synthesis. The single transmembrane segment peptide of **AI** (designated $\mathbf{AI_{pep}}$) (sequence KKKKKF^{8}-AIAIAIIAWA**X**^{19}AIIAIAIAI^{28}KKKKK, where **X** = I) was synthesized using Fmoc chemistry on a PerSeptive Biosystems Pioneer peptide synthesizer, using the standard (45 min) cycle (*20*). Four-fold excess amino acid on a 0.1 mmol scale was used with the HATU/DIEA activator pair. An amidated C-terminus was produced using a low-load (0.18−0.22 mmol/g) PAL−PEG−PS resin. The peptide was then cleaved using a cocktail consisting of 88% TFA/5% phenol/5% ultrapure water/2% TIPS. The cleaved peptide was subsequently precipitated with ice-cold diethyl ether, dried in a desiccator, and redissolved in ultrapure water. For purification, the $\mathbf{AI_{pep}}$ peptide (10 mg) was loaded onto a C4 preparative RP-HPLC column (Phenomenex), and the major peak from a water/acetonitrile gradient was collected and lyophilized. The molecular weight of the purified peptide was confirmed using mass spectrometry. Peptide concentrations were determined using the Micro BCA assay (Pierce).

Fluorescence Spectroscopy of $\mathbf{AI_{pep}}$ Labeled Peptides. On-resin labeling of $\mathbf{AI_{pep}}$ with dansyl (donor) and dabsyl (acceptor) onto the N-terminus of the peptide was performed after peptide synthesis. Uncleaved resin was reacted with a 10-fold excess of the sulfonyl chloride derivatives of dansyl or dabsyl in a minimal amount of 5% DIEA/95% DMF with overnight incubation. Peptides were then cleaved and purified as described above. The molecular weights of the dansyl- and dabsyl-labeled $\mathbf{AI_{pep}}$ were determined using mass spectrometry, and peptide concentrations were determined using the Micro BCA assay (Pierce).

FRET experiments were carried out using dansyl-labeled $\mathbf{AI_{pep}}$ (donor) in the presence of increasing mole fractions of dabsyl-labeled $\mathbf{AI_{pep}}$ (acceptor). The dansyl-labeled $\mathbf{AI_{pep}}$ concentration was maintained at 1 μM as the mole fraction of dabsyl-labeled $\mathbf{AI_{pep}}$ was increased. Experiments were conducted in 20 mM SDS and 20 mM Tris−HCl, pH 8.0. The emission wavelength was set at 341 nm, and emission spectra were collected from 450 to 650 nm. FRET competition experiments with $\mathbf{AI_{pep}}$ in SDS were conducted with 2 μM dansyl-labeled $\mathbf{AI_{pep}}$ alone, a 1:1 mixture of dansyl (donor)-labeled $\mathbf{AI_{pep}}$ and dabsyl (acceptor)-labeled $\mathbf{AI_{pep}}$, a mixture of donor/acceptor/unlabeled $\mathbf{AI_{pep}}$ (1:1:2), or a mixture of donor/acceptor/unlabeled HsmR TM1 (1:1:2). All FRET competition experiments were performed in the presence of 20 mM SDS and 20 mM Tris−HCl, pH 8.0, with the emission wavelength set at 341 nm and emission spectra collected from 450 to 650 nm.

TOXCAT Chimera Construction. The expression vectors pccKAN, pccGpA-wt, and pccGpA-G83I, along with *E. coli* strain NT 326, were kindly provided by Dr. Donald Engelman, Yale University. The TOXCAT constructs consist of an N-terminal DNA-binding domain of ToxR, a transmembrane domain, and the periplasmic maltose-binding protein (*21*). Oligonucleotides encoding the single transmembrane segment of **AI** (sequence F^{8}AIAIAIIAWA**X**^{19}AIIAIAIAI^{28}, where **X** = I) was restriction digested with *Nhe*I and *Bam*HI and ligated into the *Nhe*I and *Bam*HI sites of the restriction-digested plasmid pccKAN. The sequence of the **AI** (single TM)−TOXCAT chimera was confirmed using DNA sequencing. The resulting plasmids were transformed into NT 326 (*malE*$^{-}$) cells for further analysis. Whole cell lysates were used to estimate expression levels of the constructs. Samples were run on SDS−PAGE, followed by Western blot analysis using an antibody against MBP (NEB). Blots were developed using goat anti-rabbit HRP secondary antibody (Sigma). The correct orientation of the constructs (i.e., MBP located in the periplasm) was confirmed by growth on minimal medium containing 0.4% maltose as the only carbon source.

CAT Assays. A 200 μL sample of cells at an A_{600} of 0.6 were pelleted and resuspended in 500 μL of 0.1 M Tris−HCl, pH 8.0. The cells were lysed by addition of 20 μL of 100 mM EDTA, 100 mM dithiothreitol, 50 mM Tris−HCl, pH 8.0, and one drop of toluene, and incubated at 30 °C for 30 min. The cell-free extracts were then incubated at 37 °C with [^{3}H]chloramphenicol and *n*-butyryl coenzyme A for 90 min. The reaction was halted by partitioning the [^{3}H]-chloramphenicol−butyryl-CoA complex into xylene. The organic phase was subsequently washed and quantified using the radiolabel. All measurements were performed in triplicate, and errors shown are standard deviations on three measurements.

Molecular Modeling. Energy-minimized models of the interaction between TM helices corresponding to residues 8−29 (TM 1) and 34−55 (TM 2) of the **AI** construct were produced using a global conformation search program as described (*22*). The program identifies energetically favorable packing interfaces between paired TM helices, analyzes all possible interactions between two helices defined by the user, and then returns sets of probable structures. The connecting loop (SPGS) was not included in the simulation.

RESULTS

De Novo Design of Hydrophobic Helical Hairpins. To explore the tertiary contacts between TM helices, we designed and expressed in *E. coli* hydrophobic helix−loop−helix constructs (prototypic sequence K^{1}KKKKKKFAI-AIAIIAWA**X**^{19}AIIAIAIAIKSPGSKIAIAIAIIA**Z**^{44}AWAI-

IAIAIAFKKKKKKK[62]). Envisioned as a hydrophobic helical hairpin, this sequence (termed "**AI**") represents the minimal tertiary model of folding for two antiparallel α-helices in the lipid domain of a membrane protein. The sequence incorporates several specific features (Figure 1) (*23*, *24*). Each of the two helices consists of alternating small (Ala) and large (Ile) residues chosen to maximize interhelical tertiary contacts through van der Waals packing (*25*). As well, these residues are of sufficient hydrophobicity to ensure that each potential TM segment was well above the threshold value for spontaneous membrane insertion (*1*, *26*). Other key features include (i) "Lys-tags" on both termini to promote aqueous solubility during earlier steps in the expression protocols (*27*, *28*), (ii) a Trp residue in the center of each helix (to act as a fluorescent probe of insertion into micelles), and (iii) a Phe residue at the end of each helix (to act as an "anchor" at the presumed water−lipid interface) (*29*). A soluble loop was positioned between the two putative TM segments, which included Pro and Gly residues, since these amino acids have high β-turn propensities according to Chou−Fasman rules (*29*, *30*). Finally, a guest residue was included in each helix (denoted by **X** (Ile 19; N-terminal helix) and **Z** (Ile 44; C-terminal helix)). To the extent that could be anticipated in the initial design, these residues were strategically placed so that they were likely across from each other, and ideally present at the interface between the two helices in the folded hairpin.

*Insertion of the **AI** Construct into Micellar Membranes.* The highly hydrophobic nature of these constructs generally precluded their isolation in quantities amenable to biophysical analysis. However, following expression, cleavage of the Trx fusion protein by thrombin, and purification on a preparative scale (see the Experimental Procedures), the CD spectra of the **AI** construct (Figure 1) exhibited minima at 208 and 222 nm (ellipticity at 208 nm ca. −28000°) in a micelle environment (SDS) (Figure 2a)—an indicator of helical structure and membrane insertion (*6*, *9*, *17*, *19*, *27*). Fluorescence spectroscopy performed on the purified **AI** construct revealed a blue shift (with accompanying intensity increase) in the Trp emission maximum from 330 nm in aqueous buffer (suggesting some preexisting "burial" of Trp) to 320 nm in a micellar environment, providing a further indication of membrane insertion (Figure 2b).

*Packing Affinity between the TM Segments of the **AI** Hairpin.* While the **AI** construct is expected to be folded into a hairpin via favorable van der Waals packing of large (Ile) and small (Ala) hydrophobic side chains, we sought independent confirmation of the high affinity of the two **AI** TM segments. In this context, two independent methods were employed: a study of the oligomeric state(s) of a peptide corresponding to a single TM segment of **AI** (termed $\mathbf{AI_{pep}}$) and the use of the corresponding single **AI** TM segment in the TOXCAT dimerization assay (*21*).

The oligomeric state of $\mathbf{AI_{pep}}$ was probed using SDS−PAGE analysis. Varying amounts (from 37.5 to 7500 ng) of the single TM peptide (monomeric MW = 3404.4) were loaded onto a 12% NuPage gel and analyzed by silver staining (Figure 3a) and Coomassie blue staining (Figure 3b). Throughout this large concentration range, $\mathbf{AI_{pep}}$ migrates within a region expected for an SDS-resistant dimer. Thus, when loaded at the concentration typically used for standard SDS−PAGE analysis (Figure 3b, lane 4), $\mathbf{AI_{pep}}$ (net charge = +10) migrates at a MW = 2.16 vs its monomeric molecular weight (where the value of 2.16 = MW observed on the gel divided by the actual peptide dimer MW). This value is consistent with an earlier systematic study of glycophorin A (GpA) peptide dimers tagged with increasing numbers of Lys residues, where corresponding MWs observed on the gel vs the actual GpA peptide dimer MW were 1.90 (net charge = +6), 1.98 (+8), 2.18 (+10), and 2.58 (+12) [*28*]. The present result strongly suggests that the two TM helices within the **AI** hairpin have a high affinity for each other, even at very low concentrations, and likely pack together tightly via a unique interface containing a network of van der Waals interactions. Independent of the above analysis, the gradual linear increase in apparent molecular weight noted for the $\mathbf{AI_{pep}}$ dimer in Figure 3a,b as the loading concentration is increased through a 200-fold range is likely attributable to a mass action effect of heavier loading.

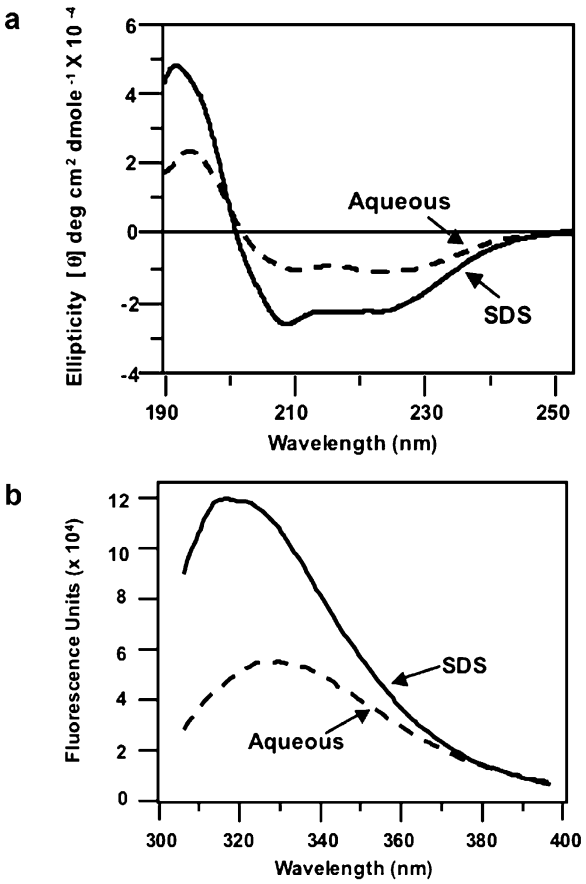

FIGURE 2: Circular dichroism and tryptophan fluorescence spectral analyses of the **AI** (**X**/**Z** = I/I) construct. (a) CD spectra obtained for the **AI** construct in either an aqueous (dotted line) or an SDS (solid line) environment. Lyophilized protein was resuspended at a final concentration of 10 μM in either 20 mM Tris−HCl, pH 8.0, or 20 mM Tris−HCl, pH 8.0, containing 34 mM SDS. (b) Trp fluorescence spectra obtained for the **AI** construct in either an aqueous (dotted line) or an SDS (solid line) environment. Lyophilized protein was resuspended at a final concentration of 2 μM in either 20 mM Tris−HCl, pH 8.0, or 20 mM Tris−HCl, pH 8.0, containing 6.8 mM SDS.

To further confirm that the oligomeric state of $\mathbf{AI_{pep}}$ was dimeric, a set of FRET experiments was conducted using donor-labeled dansyl peptides and acceptor-labeled dabsyl peptides. The stoichiometry of association for an oligomer can be determined by measuring the relative fluorescence yield (F/F_o) of donor dansyl-$\mathbf{AI_{pep}}$ as a function of the

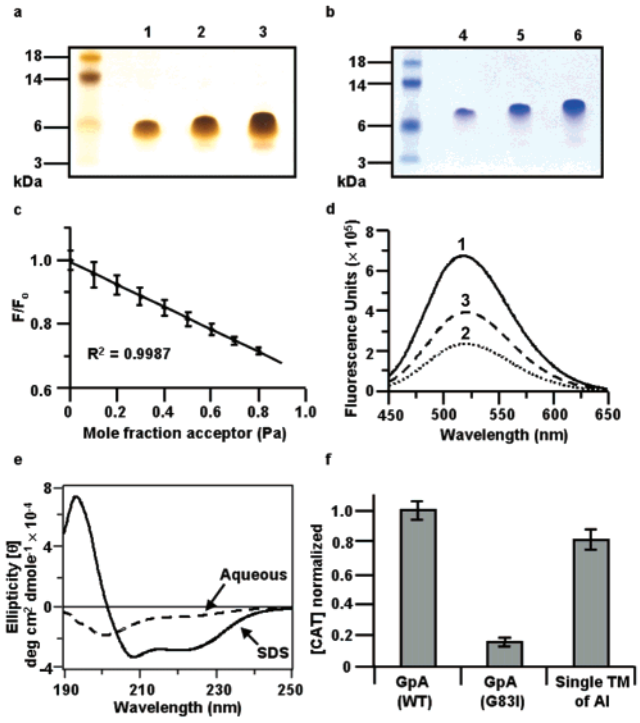

FIGURE 3: In vitro and in vivo analyses of the single TM of the **AI** hairpin. (a) Purified $\mathbf{AI}_{pep}$ peptide (sequence KKKKKFAIAIAI-IAWAIAIIAIAIAIKKKKK; 3404.4 Da) analyzed by SDS−PAGE on a 12% NuPage−bis-tris gel, and developed by silver staining. (b) Purified $\mathbf{AI}_{pep}$ peptide analyzed as in (a), except the gel was stained with Coomassie blue. From left to right in gels (a) and (b), the amounts of peptide loaded are 37.5 ng (lane 1), 75 ng (lane 2), 187.5 ng (lane 3), 1500 ng (lane 4), 3000 ng (lane 5), and 7500 ng (lane 6). (c) Relative fluorescence quantum yield of donor dansyl-labeled $\mathbf{AI}_{pep}$ in the presence of increasing mole fractions of dabsyl-labeled $\mathbf{AI}_{pep}$ acceptor. The dansyl-labeled $\mathbf{AI}_{pep}$ concentration was maintained at 1 μM as the mole fraction of dabsyl-labeled $\mathbf{AI}_{pep}$ was increased. Experiments were conducted in 20 mM SDS and 20 mM Tris−HCl, pH 8.0. (d) FRET competition experiment with $\mathbf{AI}_{pep}$ in SDS. Spectra are labeled as follows: curve 1, 2 μM dansyl-labeled $\mathbf{AI}_{pep}$ alone; curve 2, 1:1 mixture of dansyl (donor)-labeled $\mathbf{AI}_{pep}$ and dabsyl (acceptor)-labeled $\mathbf{AI}_{pep}$; curve 3, mixture of donor/acceptor/unlabeled $\mathbf{AI}_{pep}$ (1:1:2). (e) CD spectra obtained for $\mathbf{AI}_{pep}$ in aqueous and SDS micellar environments, as indicated in the diagram. For sample preparation, lyophilized protein was resuspended at a final concentration of 30 μM in 20 mM Tris−HCl, pH 8.0, ± 34 mM SDS. (f) CAT activity measurements in the TOXCAT assay for a single TM sequence of **AI**. The bars indicate the amount of CAT activity normalized to the wild-type GpA dimer. Both wild-type GpA and its disruptive mutant G83I are shown for comparison. Error bars represent the standard deviation of at least three measurements for each construct.

amount of acceptor dabsyl-$\mathbf{AI}_{pep}$ (*31*, *32*, *33*). Results (Figure 3c) show that FRET spectra of the $\mathbf{AI}_{pep}$ oligomer yielded a linear relationship that fit a straight line ($R^2 = 0.9987$), which confirms that $\mathbf{AI}_{pep}$ is a dimer. Furthermore, to ensure that the association of $\mathbf{AI}_{pep}$ was specific, fluorescence spectra were obtained in the presence of unlabeled $\mathbf{AI}_{pep}$ and a control peptide, Hsmr TM1, which is known to be monomeric (*34*). When unlabeled $\mathbf{AI}_{pep}$ was added at equimolar levels with respect to the total concentration of dansyl- and dabsyl-labeled $\mathbf{AI}_{pep}$, FRET was reduced by approximately 50% (Figure 3d), indicating that the peptides have equilibrated and association is not affected specifically by the labels (*35*). In contrast, the addition of HsmR TM1 monomeric peptide did not alter FRET between the donor- and acceptor-labeled peptides (not shown). CD spectra recorded

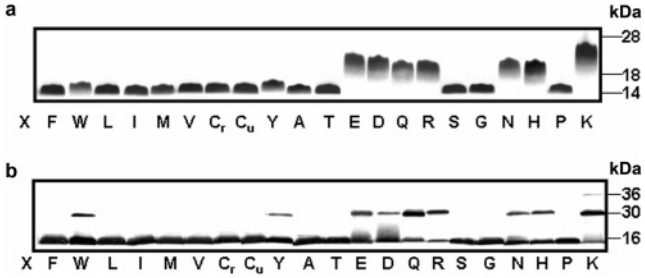

FIGURE 4: Oligomerization assays for each of the 20 commonly occurring amino acids at position **X** (Ile 19) (where **Z** = I (Ile 44) is kept constant) on different gel systems. Each mutant was lysed using the BPER reagent, and the soluble whole cell lysate was analyzed by Western blot (using S-protein HRP-conjugate) on various gel systems. The **X** = C mutant was run under both reducing and nonreducing conditions (C_r and C_u, respectively). (a) NuPage gel system (pH 6.8). (b) Tris−glycine gel system (pH 8.6).

for unlabeled $\mathbf{AI}_{pep}$ exhibited minima at 208 and 222 nm, with an ellipticity at 208 nm of ca. −33000°, indicating an essentially fully helical structure in a micelle environment (SDS) (Figure 3e) (*6*, *9*, *17*, *19*, *27*). Similar results were observed for dansyl- and dabsyl-labeled $\mathbf{AI}_{pep}$ (not shown).

To obtain an in vivo assessment of affinity between the TM helices of the **AI** hairpin, the single TM of **AI** was cloned into the TOXCAT chimera. For comparison, both glycophorin A (GpA) (WT) (a high-affinity dimer) and GpA (G83I) (a mutant that disrupts GpA dimerization) (*15*, *16*) were analyzed in parallel. Results from the TOXCAT assay (Figure 3f) demonstrate that the single **AI** TM segment dimerizes at approximately 80% vs wild-type GpA. This result provides further evidence that the TM of **AI** forms a strong dimer that inserts effectively into the *E. coli* membrane, and that the two TM helices within an individual **AI** hairpin have the innate capacity to pack effectively with one another.

Oligomerization Assays for ***X*** *Helix Mutants of the* ***AI*** *Hairpin.* Although SDS denatures some oligomeric membrane proteins (*36*, *37*), many retain their native states on SDS−PAGE gels (*7*, *8*, *10*, *11*, *15*, *16*, *38*−*43*). This method is thus very useful in the screening/comparing of mutants, as well as in estimating molecular weights (*12*). In the present work, oligomeric state(s) of thrombin-cleaved cellular lysates of a library of **AI** mutant hairpins were characterized using Western blot analysis (using an S-protein HRP-conjugate antibody). In this set of experiments, site-directed mutagenesis was first performed on the **AI** construct at the **X** residue locus, while keeping **Z** constant as Ile, to create 20 **AI** constructs. From Western blot analysis on NuPage gels (Figure 4a), it is apparent that the majority of the **X** mutants are present in the monomeric form (**X** = F, L, I, M, V, C, A, T, S, G, and P), with slightly slower migration rates noted for **X** = W and Y. However, the remaining **X** mutants (**X** = E, D, Q, R, N, H, and K) all run at rates on the Western blots (Figure 4a) tending toward the molecular weight of a dimeric species. The fact these latter seven mutants all migrate in the same direction indicates that charge effects are not the origin of the observed migration rates. In Figure 4a, the lanes containing dimeric species display migration rates likely representative of relatively rapid equilibrium between populations of monomeric and dimeric species. This situation is clarified on Tris−glycine Western blots (Figure 4b). The latter gel system puts the monomer−dimer popula-

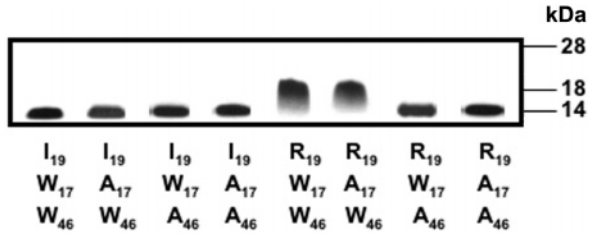

FIGURE 5: Oligomerization assays for **X** = I and R, with W17 and W46 "knockout" mutants. Each mutant was lysed using the BPER reagent, and the whole cell lysate was analyzed by Western blot (with S-protein HRP-conjugate) on the 12% NuPage− bis-tris gel system. **X** = I and **X** = R mutants were both analyzed for W17A, W46A, or both W17A and W46A. For **X** = R (also for **X** = H and K; not shown) dimer formation is eliminated for W46A or W17A/W46A, while W17A remains dimeric. There were no observable changes in migration rates for **X** = I mutants.

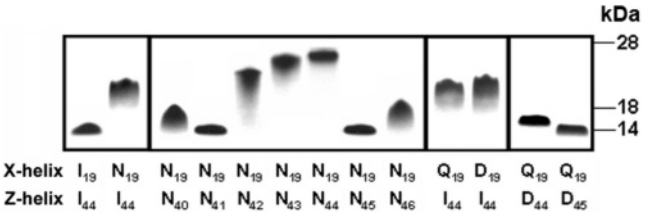

FIGURE 6: Oligomerization assays for **X** = N, Q, and D, and selected **X**/**Z** = N/N mutants (while **X** is held constant as Asn) and Q/D mutants. **Z** = Asn was walked from position **Z** − 4 (Ala 40) (where "−" denotes positions upstream of **Z**) to position **Z** + 2 (Trp 46) (where "+" denotes positions downstream of **Z**). Dimer formation is eliminated at **Z** + 1 (mutant I19N/A45N) and **Z** − 3 (mutant I19N/I41N) positions. Two further mutants (I19Q/I44D and I19Q/A45D) are shown, with their migration rates compared with those obtained for the N/N **X**/**Z** constructs. Western blots were prepared as described in Figure 4.

tions into slow equilibrium, so that the two species are resolved. With a net positive charge of +11 on the **AI** monomer and most **X** analogues, their migration rate near MW = 14000 (equivalent to ca. 1.25 times the **AI** (**X** = I) monomer MW of 11120) (Figure 4) equates to a value of ca. 2.50 for the **AI** dimer, a value within the range observed for peptide dimers of similar positive charge (*28*) (vide infra).

Four of the seven slower migrating **X** mutants (**X** = E, D, Q, and N) likely form "four-helix" structures by pairing two hairpins through side chain−side chain H-bonds (see the Discussion). However, since the remaining three slower migrating **X** mutants (**X** = R, H, and K) must also dimerize by pairing two hairpins, the possibility arose that dimer stabilization in these instances was attributable to cation−π interactions (*44*), given the availability of Trp in both the **X** and **Z** helices in the construct design. To examine the mechanism by which the basic **X** substitutions dimerize, several further mutants were constructed. The role of Trp in the dimerization of **X** = R, H, and K was probed by creating each of the basic **X** residue constructs with W17, W46, or both W17 and W46 residues mutated to Ala. These mutants were then analyzed by Western blot (Figure 5) as described above. Our results showed that, for **X** = R, the W17A mutant remains dimeric, whereas W46A and W17A/W46A mutants return to a monomeric migration rate. Similar migration patterns were observed for **X** = H and **X** = K mutants (data not shown). Also, no migration changes on Western blot were observed for Trp mutants in the **AI** construct (I19/I44).

Oligomerization Assays for X/Z Double Mutants. To assess in greater detail the molecular origin of dimer formation in several **X** mutants, a further library of **X**/**Z** double mutants was constructed. An initial double mutant created was the **X**/**Z** = I19N/I44N mutant. It might be hypothesized that this mutant should be monomeric because it appears structurally disposed to the creation of an interhelical H-bonded hairpin (between **X** and **Z** helices within one hairpin) rather than an interhairpin four-helix bundle. However, analysis of this mutant by Western blot (Figure 6) revealed that the I19N/I44N mutant actually stabilizes dimer formation. Given that this mutant did not form an "intrahairpin" hydrogen bond, the question arose as to whether the **X** and **Z** positions are actually positioned optimally within the **AI** TM−TM interface. It is possible that, in a tightly folded hairpin, the **X** and/or **Z** side chains could be facing away from the interface, such that intrahairpin H-bond formation would require an induced "twist" around at least one of the helical major axes to form the interfacial H-bond. In the absence of such a twist—ostensibly prevented by strong van der Waals packing—the presence of a single polar residue would likely cause hairpin dimerization, as observed in Figure 4.

To locate the positions of the **X** and **Z** residues relative to the interface in the **AI** construct, a scanning mutagenesis approach was used for the **AI** construct where **X** was held constant (at **X** = N) while **Z** (where **Z** = N) was "walked" approximately one turn above (−**Z** direction) and one turn below (+**Z** direction) its original position along the helix, encompassing the region A^{40}II**A**I**A**W^{46}. It was reasoned that if the relative positioning of the original **X** and **Z** residues was incompatible, dimer formation would be abrogated when favorable interfacial positions became available. The results (Figure 6) confirm that the original positioning of the **Z** residue was suboptimal vis-à-vis the helix−helix interface. Instead, the **Z** + 1 (mutant I19N/A45N) and **Z** − 3 (mutant I19N/I41N) positions for Asn were favored for intrahairpin H-bond formation, as indicated by the presence of the monomer for these latter mutants. As well, the fact that dimerization was abrogated in the latter two mutants indicated that the **AI** construct was indeed folded into a helical hairpin, as further supported by the dimeric state of the single TM $\mathbf{AI}_{\mathbf{pep}}$ (Figure 3a,b). Energy-minimized molecular models of the **X**/**Z** helical dimer are consistent with a lipid-facing position of residue 44 in the **Z** helix (Figure 7).

Oligomerization States of Q/D Mutants. Previous studies from this laboratory (*6*) have shown that the cystic fibrosis phenotypic mutant V232D (TM4) in the TM 3−4 construct of CFTR (cystic fibrosis transmembrane conductance regulator) is able to form a hydrogen bond with a wild-type Gln-(Q207) residue in the adjacent transmembrane segment (TM3). Thus, **X**/**Z** = I19Q/I44D was prepared to test whether formation of a similar intramolecular hydrogen bond occurs in the context of the **AI** construct. In this case (Figure 6), the Q/D couplet is able to form such an intrahairpin H-bond, which is signaled by its migration position at near-monomer. These results provided an indication that the formation of either intra- or interhairpin hydrogen bonds in the **AI** construct is highly residue- and context-dependent. Given the interfacial positioning of the **X** and **Z** residues determined above, the I19Q/A45D mutant was prepared for comparison to the I19Q/I44D mutant. Results indicate that with D at position 45, this mutant similarly migrates as a monomer

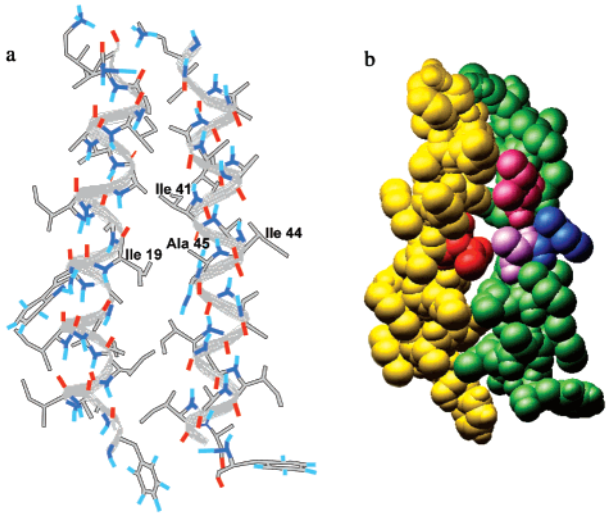

FIGURE 7: Energy-minimized molecular models of the **AI** construct. Models were generated using a global conformation search program as described (*18*). (a) Backbone model with **X** (Ile-19), **Z** (Ile-44), **Z** + 1 (Ala-45), and **Z** − 3 (Ile-41) residues highlighted. (b) Space-filling model with **X** (red), **Z** (blue), **Z** + 1 (purple), and **Z** − 3 (pink) residues highlighted. The **X** helix is colored in yellow; the **Z** helix is colored in green.

(Figure 6)—but at a discernibly more "monomeric" rate than the D44 system. This faster migration rate provides further evidence for optimal intrahairpin H-bond formation at the **Z** + 1 position.

DISCUSSION

Studies of the residue-mediated oligomerization states formed by designed hydrophobic helical hairpin constructs were performed to progress toward a set of rules for the folding of helical membrane proteins, and provide insights into the relative contributions of van der Waals packing at TM helix−helix interfaces, and hierarchical H-bonding potentials within membranes among various polar residues. Evidence that the two TM segments in the **AI** construct contain an interface conducive for folding into a hairpin structure was obtained from the results that (i) the single TM $\mathbf{AI}_{pep}$ peptide derived from the **AI** hairpin has high affinity for itself, forming stable dimers on SDS−PAGE and FRET, and (ii) the corresponding single TM sequence forms dimers almost as stable as glycophorin A when examined in vivo in TOXCAT assays (Figure 3). The fact that the single **AI** TM segment forms strong uniquely dimeric species suggests the presence of a preferred helix−helix interface, possibly mediated by the copresence in the linear sequence of three AxxxA "motifs" which—similar to GxxxG motifs—may be expected to promote interhelical packing (*45*, *46*).

As it was our intention to create constructs that were certain to be membrane-interactive, and were likely to fold into hairpin structures via strong van der Waals interfacial packing interactions, the original design involved the use of highly hydrophobic sequences, rich in Ala and Ile. This situation rendered the resulting constructs largely water-insoluble (despite the incorporation of Lys-tags (*9*, *17*, *27*, *28*)), and resistant to purification attempts from both soluble fractions and inclusion bodies. As such, it was not routinely feasible to isolate these constructs in amounts suitable for biophysical analysis; the basic **AI** construct displays CD and fluorescence spectra indicative of membrane insertion (Figure 2). This situation necessitated the use of Western blot analyses reported here, and it should be noted that, since these analyses are performed directly after cleavage of cell lysates with thrombin, **AI** constructs were generally examined in the copresence of a mixture of *E. coli* proteins.

*Oligomerization Assays for **X** and **X/Z** Mutants of the **AI** Construct.* Examination of the 20 **X** residue **AI** hairpin mutants in the Tris−glycine gel system (Figure 4b) allowed for observation of separate monomeric and dimeric species in ratios reflecting their migration positions in Figure 4a. Polar side chains likely drive the dimerization of two helical hairpins together by partnering to form H-bonded four-helix bundle-type structures (**X** = E, D, Q, and N); in these instances, it becomes energetically favorable to "bury" the pairs of polar residues between two **X** helices.

Of particular interest were **X/Z** pairs of strongly polar residues, where it might initially be expected that all combinations of the strongly polar residues (Asp, Glu, Asn, and Gln) would preferentially form an **X**−**Z** intrahairpin H-bond. However, for **X/Z** = I19N/I44N, dimer formation was actually stabilized, whereas for **X/Z** = I19Q/I44D, the migration returned to a largely monomeric position (Figure 6). These phenomena originate from the fact that the Z44 side chain projects partially outward toward lipid (Figure 7), such that the I19N/I44N pair may not be within intramolecular H-bonding distance, yet the longer Q19 side chain may nevertheless be able to "capture" the D44 side chain. In this context, Asn-scanning mutagenesis performed to generate a library of Asn mutants ranging from **Z** − 4 (Ala 40) to **Z** + 2 (Trp 46) (Figure 6) indeed showed that the **Z** + 1 (mutant I19N/A45N) and the **Z** − 3 (mutant I19N/I41N) positions are optimally positioned for intrahairpin H-bond formation between two Asn residues. These results also support the notion that the construct is properly folded into a helical hairpin, that the extant packing between the two helices in the **AI** construct is tight, and that there is essentially no free rotation of the helices around their central axes.

Oligomeric State of Constructs Containing Basic Residues. A novel finding from this work is that **X** = R, H, and K are able to form dimers on Western blot analysis, raising the possibility that dimerization was occurring through cation−π interactions involving neighboring Trp-17 and/or Trp-46 residues. Cation−π interactions involving tryptophan are well documented; some examples include ligand binding to receptors (i.e., acetylcholine to the acetylcholine receptor and acetylcholine esterase), as well as stabilization of protein structure (i.e., glucoamylase (PDB code 1GAI) contains a Lys residue surrounded by four aromatic residues) (*44*, *47*−*49*). Western blot analysis of a series of Trp knockout mutants (Figure 5) indicated that **X** = R, H, and K with either W46A or W17A/W46A were monomeric, whereas W17A remained dimeric. These findings provide strong evidence that dimerization is mediated in each construct via (likely two) pairs of basic residue−Trp-46 interactions. This situation would allow the basic residue to remain charged within the membrane, with its positive charge further shielded through interactions within the four-helix interface. These experiments appear to exclude the possibility that a hairpin dimer arises via pairing of two uncharged Lys side chains within the micelle environment to form an −N−H···N−

linkage. Similar experimental results were obtained for His- and Lys-containing species (not shown). In a related vein, the small percentage of dimer noted for the **X** = W and **X** = Y mutants (Figure 4) likely arises from "weakly polar" aromatic−aromatic interactions between W19 or Y19 and W46 (*50*).

*Proposed Folding Model for the **AI** Construct.* In the context of a tightly van der Waals-stabilized helical hairpin, intrahairpin H-bonding will not occur when a "strongly polar" **X** residue does not have an interfacially positioned "polar partner" on the **Z** helix, and therefore, its H-bonding potential must be satisfied in an alternative manner. For the single **X** mutants where X = E, D, Q, or N, the **AI** oligomerization state appears similar to previously designed single TM model systems (*7*, *8*, *10*, *11*), except here side chain−side chain H-bond formation occurs *between* two hairpins. Thus, it is likely that these **X** substitutions are able to adopt rotamers that would project away from the **AI** interface, where they become available for the formation of four-helix species. It should be emphasized that neither the Western blot analyses nor the modeling procedures can provide any specific conformational details of the relative orientation (i.e., parallel and/or antiparallel) of the interhairpin packing motifs in the four-helix species.

The overall findings suggest that mutation type and position strongly modulate the competition between interhelical interactions within a single helix−loop−helix structure vs the formation of oligomeric interactions between helices on separate constructs. In developing a unifying conceptualization to explain our results, it appears that van der Waals interactions are the dominating force in the folding of the **AI** construct (Figure 7). If this assumption is correct, then an intrahairpin H-bond will arise in these systems only if its formation provides additional stability over the total energy contribution of the existing van der Waals interactions. This finding provides an interesting complement to previous work in this laboratory on polar substitutions within the TM3/4 construct of CFTR (*6*). In the TM3/4 construct, the total energy contribution for the van der Waals interactions is estimated to be relatively low, as hairpins were observed to run as "open" monomeric structures on SDS−PAGE. Nevertheless, introduction of a CF-phenotypic mutant (V232D) into the CFTR TM3/4 hairpin construct produces a H-bond between wild-type Gln-207 (TM3) and Asp-232 (TM4) residues to drive—and lock—the two helices together as an "SDS-resistant" folded pair (*6*). In fact, the average hydrophobicity of the **X** and **Z** helices in **AI** is much higher than that of CFTR TM helices 3 and 4 (*19*), and it appears that, in **AI** systems, hydrophobic packing *alone* produces such SDS-resistant folded structures—which in turn mitigates against rotational freedom about the major **AI** helix axes. Thus, introduction of paired polar substituents produces the strongest H-bonds only when **X** and **Z** ($\pm n$) positions are interfacial and relatively proximal—a situation further nuanced by structural differences-in-detail among the side chains of Asp, Glu, Asn, and Gln. The fact that the **AI** construct produced van der Waals packing energies ostensibly higher than, e.g., those of the CFTR TM3/4 hairpin, suggests that a given multispanning domain of a membrane protein could well contain examples of both "loosely" and "tightly" packed helices as required for function. The present results highlight the importance of the balance between two of the key determinants in helix−helix interfacial motifs, viz., van der Waals packing and side chain−side chain H-bond formation, and suggest scenarios where this balance could become tipped in misfolded or disease states of membrane proteins.

ACKNOWLEDGMENT

We thank Dr. Alex Therien for conceptual contributions and Ms. Nur Muhammed-Ally for excellent technical assistance in the early phases of this research.

REFERENCES

1. Liu, L.-P., and Deber, C. M. (1998) Guidelines for membrane protein engineering derived from *De novo* designed model peptides, *Biopolymers 47*, 41−62.
2. Popot, J.-L., and Engelman, D. M. (1990) Membrane protein folding and oligomerization: The two-stage model, *Biochemistry 29*, 4031−4037.
3. Popot, J.-L., and Engelman, D. M. (2000) Helical membrane protein folding, stability, and evolution, *Annu. Rev. Biochem. 69*, 881−922.
4. Bowie, J. U. (1997) Helix packing in membrane proteins, *J. Mol. Biol. 272*, 780−789.
5. Javadapour, M. M., Eilers, M., Groesbeek, M., and Smith, S. O. (1999) Helix packing in polytopic membrane proteins: Role of glycine in transmembrane helix association, *Biophys. J. 77*, 1609−1618.
6. Therien, A. G, Grant, F. E., and Deber, C. M. (2001) Interhelical hydrogen bonds in the CFTR membrane domain, *Nat. Struct. Biol. 8*, 597−601.
7. Choma, C., Gratkowski, H., Lear, J. D., and DeGrado, W. F. (2000) Asparagine-mediated self-association of a model transmembrane helix, *Nat. Struct. Biol. 7*, 161−166.
8. Gratkowski, H., Lear, J. D., and DeGrado, W. F. (2001) Polar side chains drive the association of model transmembrane peptides, *Proc. Natl. Acad. Sci. U.S.A. 98*, 880−885.
9. Partridge, A. W., Melnyk, R. A., and Deber, C. M. (2002) Polar residues in membrane domains of proteins: Molecular basis for helix-helix association in a mutant CFTR transmembrane segment, *Biochemistry 41*, 3647−3653.
10. Zhou, F. X., Cocco, M. J., Russ, W. P., Brunger, A. T., and Engelman, D. M. (2000) Interhelical hydrogen bonding drives strong interactions in membrane proteins, *Nat. Struct. Biol. 7*, 154−160.
11. Zhou, F. X., Merianos, H. J., Brunger, A. T., and Engelman, D. M. (2001) Polar residues drive association of polyleucine transmembrane helices, *Proc. Natl. Acad. Sci. U.S.A. 98*, 2250−2255.
12. DeGrado, W. F., Gratkowski, H., and Lear, J. D. (2003) How do helix-helix interactions help determine the folds of membrane proteins? Perspectives from the study of homo-oligomeric helical bundles, *Protein Sci. 12*, 647−665.
13. Russ, W. P., and Engelman, D. M. (2000) The GxxxG motif: A framework for transmembrane helix-helix association, *J. Mol. Biol. 296*, 911−919.
14. Dawson, J. P., Weinger, J. S., Engelman, D. M., and Sturgis, J. N. (2002) Motifs of serine and threonine can drive association of transmembrane helices, *J. Mol. Biol. 316*, 799−805.
15. Lemmon, M. A., Flanagan, J. M., Hunt, J. F., Adair, B. D., Bormann, B.-J., Dempsey, C. E., and Engelman, D. M. (1991) Glycophorin A dimerization is driven by specific interactions between transmembrane α-helices, *J. Biol. Chem. 267*, 7683−7689.
16. Lemmon, M. A., Treutlein, H. R., Adams, P. D., Brunger, A. T., and Engelman, D. M. (1994) A dimerization motif for transmembrane α-helices, *Nat. Struct. Biol. 1*, 157−163.
17. Melnyk, R. A., Partridge, A. W., and Deber, C. M. (2002) Transmembrane domain mediated self-assembly of major coat protein subunits from Ff bacteriophage, *J. Mol. Biol. 315*, 63−72.
18. Melnyk, R. A., Kim, S., Curran, A. R., Engelman, D. M., Bowie, J. U., and Deber, C. M. (2004) The affinity of GxxxG motifs in transmembrane helix-helix interactions is modulated by long-range communication, *J. Biol. Chem. 279*, 16591−16597.

19. Peng, S., Liu, L.-P., Emili, A. Q., and Deber, C. M. (1998) Cystic fibrosis transmembrane conductance regulator: Expression and helicity of a double membrane-spanning segment, *FEBS Lett. 431*, 29−33.
20. Liu, L. P., and Deber, C. M. (1997) Anionic phospholipids modulate peptide insertion into membranes, *Biochemistry 36*, 5476−5482.
21. Russ, W. P., and Engelman, D. M. (1999). TOXCAT: A measure of transmembrane helix association in a biological membrane, *Proc. Nat. Acad. Sci. U.S.A. 96*, 863−868.
22. Adams, P. D., Arkin, I. T., Engelman, D. M., and Brunger, A. T. (1995) Computational searching and mutagenesis suggest a structure for the pentameric transmembrane domain of phospholamban, *Nat. Struct. Biol. 2*, 154−162.
23. Whitley, P., Nilsson, I., and von Heijne, G. (1994) *De novo* design of integral membrane proteins, *Struct. Biol. 1*, 858−862.
24. Wimley, W. C., and White, S. H. (2000) Designing transmembrane α-helices that insert spontaneously, *Biochemistry 39*, 4432−4442.
25. Langosch, D., and Heringa, J. (1998) Interactions of transmembrane helices by a knobs-into-holes packing characteristic of soluble coiled coils, *Proteins: Struct., Funct., and Genet. 31*, 150−159.
26. Deber, C. M., Wang, C., Liu, L.-P., Prior, A. S., Agrawal, S., Muskat, B. L., and Cuticchia, A. J. (2001) TM finder: A prediction program from transmembrane protein segments using a combination of hydrophobicity and nonpolar phase helicity scales, *Protein Sci. 10*, 212−219.
27. Melnyk, R. A., Partridge, A. W., and Deber, C. M. (2001) Retention of native-like oligomerization states in transmembrane segment peptides: Application to the *Escherichia coli* aspartate receptor, *Biochemistry 40*, 11106−11113.
28. Melnyk, R. A., Partridge, A. W., Yip, J., Wu, Y., Goto, N. K., and Deber, C. M. (2003) Polar residue tagging of transmembrane peptides, *Biopolymers (Pept. Sci.) 71*, 675−685.
29. Landolt-Marticorena, C., Williams, K. A., Deber, C. M., and Reithmeier, R. A. (1993) Non-random distribution of amino acids in the transmembrane segments of human type I single span membrane proteins, *J. Mol. Biol. 229*, 602−608.
30. Monne, M., Nilsson, I., Elofsson, A., and von Heijne, G. (1999) Turns in transmembrane helices: Determination of the minimal length of a "helical hairpin" and derivation of a fine-grained turn propensity scale, *J. Mol. Biol. 293*, 807−814.
31. Adair, B. D., and Engelman, D. M. (1994) Glycophorin A helical transmembrane domains dimerize in phospholipids bilayers: a resonance energy transfer study, *Biochemistry 33*, 5539−5544.
32. Li, M., Reddy, L. G., Bennett, R., Silva, N. D., Jr., Jones, L. R., and Thomas, D. D. (1999) A fluorescence energy transfer method for analyzing protein oligomeric structure: application to phospholamban, *Biophys. J. 76*, 2587−2599.
33. Veatch, W., and Stryer, L. (1977) The dimeric nature of the gramicidin A transmembrane channel: conductance and fluorescence energy transfer studies of hybrid channels, *J. Mol. Biol. 283*, 489−506.
34. Ninio, S., and Schuldiner, S. (2003). Characterization of an archaeal multidrug transporter with a unique amino acid composition, *J. Biol. Chem. 278*, 12000−12005.
35. Fisher, L. E., Engelman, D. M., and Sturgis, J. N. (1999) Detergents modulate dimerization, but not helicity, of the glycophorin A transmembrane domain, *J. Mol. Biol. 293*, 639−651.
36. Lau, F. W., and Bowie, J. U. (1997) A method for assessing the stability of a membrane protein, *Biochemistry 36*, 5884−5892.
37. Chen, J., and Gouaux, E. (1999) Probing the folding and unfolding of wild-type and mutant forms of bacteriorhodopsin in micellar solutions: Evaluation of reversible unfolding conditions, *Biochemistry 38*, 15380−15387.
38. Fujii, J., Maruyama, K., Tada, M., and MacLennan, D. H. (1989) Expression and site-specific mutagenesis of phospholamban. Studies on residues involved in phosphorylation and pentamer formation, *J. Biol. Chem. 264*, 12950−12955.
39. Vorherr, T., Wrzosek, A., Chiesi, M., and Carafoli, E. (1993) Total synthesis and functional properties of the membrane-intrinsic protein phospholamban, *Protein Sci. 2*, 339−347.
40. Simmerman, H. K., Kobayashi, Y. M., Autry, J. M., and Jones, L. R. (1996) A leucine zipper stabilizes the pentameric membrane domain of phospholamban and forms a coiled-coil structure, *J. Biol. Chem. 271*, 5941−5946.
41. Arkin, I. T., Adams, P. D., Brunger, A. T., Aimoto, S., Engelman, D. M., Rothschild, K. J., and Smith, S. O. (1997) Structure of the transmembrane cysteine residues in phospholamban, *J. Membr. Biol. 155*, 199−206.
42. Karim, C. B., Stamm, J. D., Karim, J., Jones, L. R., and Thomas, D. D. (1998) Cysteine reactivity and oligomeric structures of phospholamban and its mutants, *Biochemistry 37*, 12074−12081.
43. Splitt, H., Meuser, D., Borovok, I., Betzler, M., and Schrempf, H. (2000) Pore mutations affecting tetrameric assembly and functioning of the potassium channel KcsA from *Streptomyces lividans*, *FEBS Lett. 472*, 83−87.
44. Beene D. L., Brandt G. S., Zhong W., Zacharias N. M., Lester H. A., and Dougherty D. A. (2002) Cation-π interactions in ligand recognition by serotonergic (5-HT3A) and nicotinic acetylcholine receptors: the anomalous binding properties of nicotine, *Biochemistry 41*, 10262−10269.
45. Kleiger, G., and Eisenberg, D. (2002) GxxxG and GxxxA motifs stabilize FAD and NAD(P)-binding Rossmann folds through C(alpha)-H... O hydrogen bonds and van der waals interactions, *J. Mol. Biol. 323*, 69−76.
46. Senes, A., Gerstein, M., and Engelman, D. M. (2000) Statistical analysis of amino acid patterns in transmembrane helices: the GxxxG motif occurs frequently and in association with beta-branched residues at neighboring positions, *J. Mol. Biol. 296*, 921−936.
47. Gallivan, J. P., and Dougherty, D. A. (1999) Cation-π interactions in structural biology, *Proc. Natl. Acad. Sci. U.S.A. 96*, 9459−9464.
48. Dougherty, D. A. (1996) Cation-π interactions in chemistry and biology: A new view of benzene, Phe, Tyr, and Trp, *Science 271*, 163−168.
49. Zacharias, N., and Dougherty, D. A. (2002) Cation-π interactions in ligand recognition and catalysis, *Trends Pharmacol. Sci. 23*, 281−287.
50. Burley, S. K., and Petsko, G. A. (1985) Aromatic-aromatic interaction: a mechanism of protein structure stabilization, *Science 229*, 23−28.

BI0492760